OPTIMIZED SCHWARZ METHODS FOR THE STOKES-DARCY COUPLING

MARCO DISCACCIATI[1] AND LUCA GERARDO-GIORDA[2]

Abstract. This paper studies Optimized Schwarz methods for the Stokes-Darcy problem. Robin transmission conditions are introduced and the coupled problem is reduced to a suitable interface system that can be solved using Krylov methods. Practical strategies to compute optimal Robin coefficients are proposed which take into account both the physical parameters of the problem and the mesh size. Numerical results show the effectiveness of our approach. Stokes-Darcy coupling; Domain decomposition methods; Optimized Schwarz methods; Robin interface conditions.

1. Introduction

The Stokes-Darcy problem has received a growing attention by the mathematical community over the last decade from the seminal works by [14] and [32]. The interest for this problem is not only due to its many possible applications, but also to its mathematical nature. Indeed, it is a good example of multi-physics problem where two different boundary value problems are coupled into a global heterogeneous one. To compute the approximate solution of this problem one could solve it in a monolithic way using either a direct or a suitably preconditioned iterative method. However, its multi-physics nature makes it suitable to splitting methods typical of domain decomposition techniques. These methods allow to recover the solution of the global problem by iteratively solving each subproblem separately and they thus permit to reuse software specifically developed to deal with either incompressible or porous media flows. The difficulty of this approach is to guarantee effective convergence and robustness of the iterations.

Classical Dirichlet-Neumann type methods (see [35]) for the Stokes-Darcy problem were studied in [14] and [13] showing that they may exhibit slow convergence for small values of the viscosity of the fluid and the permeability of the porous medium. A Robin-Robin method was then proposed as a possible alternative in [13] and [16]. Analogous substructuring methods based on Robin interface conditions were subsequently studied in [7, 8, 10] and, more recently, in [6] where a comparison of these different methods has been carried out. All these works show that the Robin-Robin method is more robust than the Dirichlet-Neumann one, but it is still unclear how to choose the Robin coefficients in an optimal way taking into account both the main physical parameters of the problem and the mesh size. Indeed, apparently contradictory results can be found in the literature regarding the relative magnitude of such coefficients and their dependence on the physical and computational quantities that characterize the problem and its discretization. In this work, we focus on the effective solution of the heterogeneous Stokes-Darcy problem by means of a Robin-type interface coupling between the subdomains and

we optimize the convergence properties of the coupling algorithm in the framework of Optimized Schwarz Methods.

Differently from the classical Schwarz Algorithm (see, e.g. [38, 35, 39]), based on Dirichlet transmission conditions (rather slow and very much dependent on the size of the overlap), Optimized Schwarz Algorithms are based on more effective transmission conditions and show significant improvement in terms both of robustness and of computational cost (see [17, 18, 22, 21]). In addition, whilst in general the classical Schwarz method is not convergent in the absence of overlap, Optimized Schwarz Algorithms do not suffer from such drawback, and ensure convergence also for decompositions into non-overlapping subdomains. Optimized Schwarz Methods are thus a natural framework to deal with spatial decompositions of the computational domain that are driven by a multi-physics problem as the one at hand. Originally, P.L. Lions proposed Robin conditions to obtain convergence without overlap ([33]), while in a short note on non-linear problems [28] suggested nonlocal operators for best performance. In [9], these optimal, non-local transmission conditions were developed for advection-diffusion problems, with local approximations for small viscosity, and low order frequency approximations were proposed in [34] and [12]. Optimized transmission conditions for the best performance in a given class of local transmission conditions were introduced for advection diffusion problems in [31], for the Helmholtz equation in [21], for Laplace's equation in [20] and for Maxwell's equation in [1]. For complete results and attainable performance for symmetric, positive definite problems, see [22]. The Optimized Schwarz methods were also extended to systems of partial differential equations, such as the compressible Euler equations ([18]) and the full Maxwell system (see [17]). Recently, Optimized Schwarz strategies have been proposed for the coupling of heterogeneous models, such as in Fluid-Structure Interaction problem ([24]) and in the coupling of Bidomain and Monodomain models in electrocardiology ([26]).

The paper is organized as follow. After introducing the Stokes-Darcy problem in Section 2, in Section 3 a Robin-Robin iterative method is studied. Its convergence properties are enlightened by means of Fourier analysis in the framework of Optimized Schwarz Methods, and optimal Robin parameters for the interface conditions are devised. In Section 4 the algebraic interpretation of the method is provided and numerical tests illustrate the convergence properties of the method and its robustness with respect both to mesh size and to the problem coefficients.

2. Problem setting and discretization

We consider a computational domain formed by two subregions: one occupied by a fluid, the other formed by a porous medium. More precisely, let $\Omega \subset \mathbb{R}^{\mathrm{D}}$ ($\mathrm{D} = 2, 3$) be a bounded domain, partitioned into two non-intersecting subdomains Ω_f and Ω_p separated by an interface Γ, i.e., $\overline{\Omega} = \overline{\Omega}_f \cup \overline{\Omega}_p$, $\Omega_f \cap \Omega_p = \emptyset$ and $\overline{\Omega}_f \cap \overline{\Omega}_p = \Gamma$. We suppose the boundaries $\partial\Omega_f$ and $\partial\Omega_p$ to be Lipschitz continuous. From the physical point of view, Γ is a surface separating the domain Ω_f filled by a fluid from the domain Ω_p formed by a porous medium. We assume that Ω_f has a fixed surface, i.e., we neglect the case of free-surface flows. In Fig. 1 we show a schematic representation of the computational domain. In the following, $\mathbf{n}_p$ and $\mathbf{n}_f$ denote the unit outward normal vectors to $\partial\Omega_p$ and $\partial\Omega_f$, respectively, and we have $\mathbf{n}_f = -\mathbf{n}_p$ on Γ. We suppose $\mathbf{n}_f$ and $\mathbf{n}_p$ to be regular enough and we indicate $\mathbf{n} = \mathbf{n}_f$ for simplicity of notation.

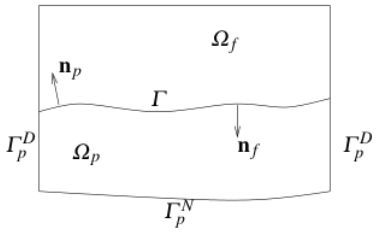

FIGURE 1. Schematic representation of a 2D section of the computational domain.

The fluid in Ω_f is incompressible with constant viscosity and density and it can be described by the dimensionless steady Stokes equations: find the fluid velocity $\mathbf{u}_f$ and pressure p_f such that

$$-\boldsymbol{\nabla} \cdot (2\mu_f \nabla^{\mathrm{s}} \mathbf{u}_f - p_f \boldsymbol{I}) = \mathbf{f}_f \quad \text{and} \quad \nabla \cdot \mathbf{u}_f = 0 \quad \text{in } \Omega_f, \tag{1}$$

where $\boldsymbol{I}$ and $\nabla^{\mathrm{s}} \mathbf{u}_f = \frac{1}{2}(\nabla \mathbf{u}_f + (\nabla \mathbf{u}_f)^T)$ are the identity and the strain rate tensor; $\mu_f = (\mathrm{Re}\,\mathrm{Eu})^{-1} > 0$ with Re and Eu being the Reynolds' and the Euler's number; $\mathbf{f}_f$ is a given external force. (∇ and $\nabla\cdot$ denote the dimensionless gradient and divergence operator with respect to the space coordinates.)

The motion of the fluid through the porous medium can be described by the dimensionless elliptic problem: find the pressure p_p such that

$$-\nabla \cdot (\boldsymbol{\eta}_p \nabla p_p) = -\nabla \cdot \mathbf{g}_p \quad \text{in } \Omega_p \tag{2}$$

where $\boldsymbol{\eta}_p = (\mathrm{Re}\,\mathrm{Eu}\,\mathrm{Da})\boldsymbol{K}$, $\boldsymbol{K}$ being the diagonal dimensionless intrinsic permeability tensor and Da the Darcy number ([3]), while $\mathbf{g}_p$ is a given external force that accounts for gravity. The fluid velocity in Ω_p can be obtained using Darcy's law (see, e.g., [2]): $\mathbf{u}_p = -\boldsymbol{\eta}_p \nabla p_p + \mathbf{g}_p$.

Suitable continuity conditions must be imposed across the interface Γ to describe filtration phenomena. As a consequence of the incompressibility of the fluid we prescribe the continuity of the normal velocity across Γ:

$$\mathbf{u}_f \cdot \mathbf{n} = -(\boldsymbol{\eta}_p \nabla p_p) \cdot \mathbf{n} + \mathbf{g}_p \cdot \mathbf{n} \quad \text{on } \Gamma. \tag{3}$$

Moreover, we impose the following condition relating the normal stresses across Γ (see, e.g., [13, 27, 32]):

$$-\mathbf{n} \cdot (2\mu_f \nabla^{\mathrm{s}} \mathbf{u}_f - p_f \boldsymbol{I}) \cdot \mathbf{n} = p_p \quad \text{on } \Gamma. \tag{4}$$

Finally, we introduce the so-called Beavers-Joseph-Saffman condition (see, e.g, [4, 37, 30, 14, 32]):

$$-((2\mu_f \nabla^{\mathrm{s}} \mathbf{u}_f - p_f \boldsymbol{I}) \cdot \mathbf{n})_\tau = \xi_f (\mathbf{u}_f)_\tau \quad \text{on } \Gamma \tag{5}$$

where $\xi_f = \alpha_{BJ}(\mathrm{Re}\,\mathrm{Eu}\sqrt{\mathrm{Da}}\sqrt{\boldsymbol{\tau} \cdot \boldsymbol{K} \cdot \boldsymbol{\tau}})^{-1}$ and α_{BJ} is a dimensionless constant which depends only on the geometric structure of the porous medium. We indicate by $(\mathbf{v})_\tau$ the tangential component of any vector $\mathbf{v}$: $(\mathbf{v})_\tau = \mathbf{v} - (\mathbf{v} \cdot \mathbf{n})\mathbf{n}$ on Γ.

As concerns the boundary conditions, several choices can be made (see, e.g., [15]). For simplicity, we consider here homogeneous boundary data and, with reference to Fig. 1 for the notation, for the Darcy problem we impose $p_p = 0$ on Γ_p^D and $\boldsymbol{\eta}_p \nabla p_p \cdot \mathbf{n}_p = \mathbf{g}_p \cdot \mathbf{n}_p$ on Γ_p^N, while for the Stokes problem we set $\mathbf{u}_f = \mathbf{0}$ on $\partial\Omega_f \setminus \Gamma$.

3. Optimized Robin-Robin method

3.1. **Formulation of the Robin-Robin method.** Let α_f and α_p be two positive parameters: $\alpha_f, \alpha_p > 0$. By combining (3) and (4) linearly with coefficients $(-\alpha_f, 1)$ and $(\alpha_p, 1)$ we obtain two Robin interface conditions on Γ:

$$-\mathbf{n}\cdot\left(2\mu_f\nabla^{\mathrm{s}}\mathbf{u}_f - p_f\boldsymbol{I}\right)\cdot\mathbf{n} - \alpha_f\mathbf{u}_f\cdot\mathbf{n} = p_p + \alpha_f\left((\boldsymbol{\eta}_p\,\nabla p_p)\cdot\mathbf{n} - \mathbf{g}_p\cdot\mathbf{n}\right), \tag{6}$$

and

$$p_p - \alpha_p\left((\boldsymbol{\eta}_p\,\nabla p_p)\cdot\mathbf{n} - \mathbf{g}_p\cdot\mathbf{n}\right) = -\mathbf{n}\cdot\left(2\mu_f\nabla^{\mathrm{s}}\mathbf{u}_f - p_f\boldsymbol{I}\right)\cdot\mathbf{n} + \alpha_p\mathbf{u}_f\cdot\mathbf{n}. \tag{7}$$

A Robin-Robin type algorithm amounts to set up a fixed point problem that solves iteratively the fluid problem with boundary condition (6) and the porous medium problem with boundary condition (7). More precisely, the algorithm reads as follows. Given the Darcy pressure p_p^0 in Ω_p, for $m \geq 1$ until convergence find the fluid velocity $\mathbf{u}_f^m$, the fluid pressure p_f^m in Ω_f and the pressure p_p^m in Ω_p such that the following problems are satisfied:

1. Stokes problem:

$$\begin{aligned}
-\boldsymbol{\nabla}\cdot(2\mu_f\nabla^{\mathrm{s}}\mathbf{u}_f^m - p_f^m\boldsymbol{I}) = \mathbf{f}_f \quad \text{and} \quad \nabla\cdot\mathbf{u}_f^m = 0 \quad & \text{in } \Omega_f \\
\mathbf{u}_f^m = \mathbf{0} \quad & \text{on } \partial\Omega_f\setminus\Gamma \\
-(\mathbf{n}\cdot(2\mu_f\nabla^{\mathrm{s}}\mathbf{u}_f^m - p_f^m\boldsymbol{I}))_\tau = \xi_f\,(\mathbf{u}_f^m)_\tau \quad & \text{on } \Gamma \\
-\mathbf{n}\cdot(2\mu_f\nabla^{\mathrm{s}}\mathbf{u}_f^m - p_f^m\boldsymbol{I})\cdot\mathbf{n} - \alpha_f\mathbf{u}_f^m\cdot\mathbf{n} = p_p^{m-1} + \alpha_f\left((\boldsymbol{\eta}_p\,\nabla p_p^{m-1})\cdot\mathbf{n} - \mathbf{g}_p\cdot\mathbf{n}\right) \quad & \text{on } \Gamma,
\end{aligned} \tag{8}$$

2. Darcy problem:

$$\begin{aligned}
-\nabla\cdot(\boldsymbol{\eta}_p\,\nabla p_p^m) = -\nabla\cdot\mathbf{g}_p \quad & \text{in } \Omega_p \\
p_p^m = 0 \quad & \text{on } \Gamma_p^D \\
-(\boldsymbol{\eta}_p\nabla p_p^m)\cdot\mathbf{n}_p + \mathbf{g}_p\cdot\mathbf{n}_p = 0 \quad & \text{on } \Gamma_p^N \\
p_p^m - \alpha_p\left((\boldsymbol{\eta}_p\,\nabla p_p^m)\cdot\mathbf{n} - \mathbf{g}_p\cdot\mathbf{n}\right) = -\mathbf{n}\cdot(2\mu_f\nabla^{\mathrm{s}}\mathbf{u}_f^m - p_f^m\boldsymbol{I})\cdot\mathbf{n} + \alpha_p\mathbf{u}_f^m\cdot\mathbf{n} \quad & \text{on } \Gamma.
\end{aligned} \tag{9}$$

We aim now to optimize the Robin-Robin algorithm (8)-(9) in the framework of Optimized Schwarz Methods. Such methods, based upon interface continuity requirements on traces and fluxes of Robin type, are a generalization of the non-overlapping algorithm proposed for elliptic problems in [33], that ensures convergence also without relaxation. Since Optimized Schwarz Methods do not require overlap to converge, they have become quite popular in the last decade, and are a natural framework to deal with a spatial decomposition of the domain driven by a multi-physics problem (see [24]). Although in general Optimized Schwarz methods based on one-sided interface conditions ($\alpha_f = \alpha_p$) have been extensively used along the years (see, e.g., [33, 22, 31, 11]), the use of two-sided interface condition ($\alpha_f \neq \alpha_p$) has recently become increasingly popular due to better convergence properties of the associated algorithms, see [1, 17, 19, 23, 25]. Since such parameters are in general obtained by suitable approximations of the symbols in the Fourier space of the Steklov-Poincaré operator (or Dirichlet-to-Neumann mapping) associated to the problem within the subdomain ([22]), the two-sided interface conditions are a natural choice in the presence of multi-physics problems where different problems have to be solved in different regions of the computational domain ([24, 26]). In the rest of the section we study, by means of Fourier analysis, the convergence properties of the Robin-Robin algorithm (8)-(9) in a simplified settings, and its optimization in the two-sided interface conditions framework.

3.2. **A simplified problem.** We introduce suitable simplifying hypotheses and subproblems. The fluid domain is the half plane $\Omega_f = \{(x,y) \in \mathbb{R}^2 : x < 0\}$, the porous medium is the complementary half plane $\Omega_p = \{(x,y) \in \mathbb{R}^2 : x > 0\}$, while the interface is given by $\Gamma = \{(x,y) \in \mathbb{R}^2 : x = 0\}$. Thus, $\mathbf{n} = (1,0)$, and $\boldsymbol{\tau} = (0,1)$. We assume μ_f to be constant, $\boldsymbol{\eta}_p = \mathrm{diag}(\eta_1, \eta_2)$ to be constant and anisotropic (i.e., $\eta_1 \neq \eta_2$), and we denote $\mathbf{u}_f(x,y) = [u_1(x,y), u_2(x,y)]^T$ and $\mathbf{g}_p = (g_1, g_2)$. In this simplified setting, the Robin-Robin algorithm reads: given $\mathbf{u}_f^0$, p_f^0, and p_p^0, solve for $m > 0$ until convergence

1. the fluid problem

(10)
$$
\begin{aligned}
-\mu_f \begin{pmatrix} (\partial_{xx} + \partial_{yy})\, u_1^m \\ (\partial_{xx} + \partial_{yy})\, u_2^m \end{pmatrix} + \begin{pmatrix} \partial_x p_f^m \\ \partial_y p_f^m \end{pmatrix} &= \mathbf{f}_f && \text{in } (-\infty, 0) \times \mathbb{R} \\
\partial_x u_1^m + \partial_y u_2^m &= 0 && \text{in } (-\infty, 0) \times \mathbb{R} \\
-\mu_f(\partial_x u_2 + \partial_y u_1) &= \xi_f\, u_2^m && \text{on } \{0\} \times \mathbb{R} \\
(-2\mu_f \partial_x u_1^m + p_f^m) - \alpha_f\, u_1^m &= p_p^{m-1} - \alpha_f\, (-\eta_1\, \partial_x p_p^{m-1} + g_1) && \text{on } \{0\} \times \mathbb{R}
\end{aligned}
$$

   (In the momentum equation we have used (1) to obtain $-\boldsymbol{\nabla} \cdot (2\nabla^{\mathrm{s}} \mathbf{u}_f) = -\Delta \mathbf{u}_f$.)

2. the porous-medium problem

(11)
$$
\begin{aligned}
-(\partial_x(\eta_1 \partial_x) + \partial_y(\eta_2 \partial_y))\, p_p^m &= -(\partial_x g_1 + \partial_y g_2) && \text{in } (0, \infty) \times \mathbb{R} \\
p_p^m + \alpha_p\, (-\eta_1\, \partial_x p_p^m + g_1) &= (-2\mu_f \partial_x u_1^m + p_f^m) + \alpha_p\, u_1^m && \text{on } \{0\} \times \mathbb{R}.
\end{aligned}
$$

3.3. **Convergence analysis.** We will base our convergence analysis on a Fourier transform in the direction tangential to the interface (corresponding to the y variable in the case at hand), which is defined, for $w(x,y) \in L^2(\mathbb{R}^2)$, as

$$
\mathcal{F} : w(x,y) \mapsto \widehat{w}(x,k) = \int_{\mathbb{R}} e^{-iky} w(x,y)\, dy,
$$

where k is the frequency variable. We will then be able to quantify the error, in the frequency space, between the normal component of the velocity at the m-th iteration, $\widehat{u}_1^m(x,k)$, and the exact value $\widehat{u}_1(x,k)$. As a consequence, we can introduce, on the interface Γ, a *reduction factor* at iteration m, for each frequency k, as

$$
\rho^m(k) := \frac{|\widehat{u}_1^m(0,k) - \widehat{u}_1(0,k)|}{|\widehat{u}_1^{m-2}(0,k) - \widehat{u}_1(0,k)|}.
$$

The Robin-Robin algorithm converges if, at each iteration m, we have $\rho^m(k) < 1$ for all the relevant frequencies of the problem, namely for $k_{min} \leq k \leq k_{max}$, where $k_{min} > 0$ is the smallest frequency relevant to the problem and k_{max} is the largest frequency supported by the numerical grid, which is of the order π/h, being h the mesh size (see [21, 22]). The ultimate goal is then to minimize, at each iteration step, the reduction factor $\rho^m(k)$ over all the Fourier modes. Note that the asymptotic requirements for the Fourier transformability of the solutions entail their boundedness at infinity.

Since the problems are linear, we can study the convergence directly on the error equation, namely the convergence to the zero solution when the forcing terms vanish, i.e. $\mathbf{f}_f = \mathbf{0}$ and $\mathbf{g}_p = \mathbf{0}$. First, we characterize the reduction factor of the algorithm.

Proposition 3.1. *Let $\eta_p = \sqrt{\eta_1 \eta_2}$. Given $\mathbf{u}_f^0, p_f^0, p_p^0$, the reduction factor of the algorithm (10)–(11) does not depend on the iteration and it is given by*

(12)
$$\rho(\alpha_f, \alpha_p, k) = |g(\alpha_f, \alpha_p, k)| \quad \textit{where} \quad g(\alpha_f, \alpha_p, k) = \left(\frac{2\mu_f\,|k| - \alpha_p}{2\mu_f\,|k| + \alpha_f}\right) \cdot \left(\frac{1 - \alpha_f\,\eta_p\,|k|}{1 + \alpha_p\,\eta_p\,|k|}\right).$$

Proof. Taking the divergence of $(10)_1$ and using $(10)_2$, the fluid problem can be rewritten in the unknown pressure

$$-\Delta p_f^{m+1} = 0 \qquad \text{in } \Omega_f.$$

Applying the Fourier transform in the y direction, the equation for the pressure above becomes, for all k, an ordinary differential equation

$$-\partial_{xx}\hat{p}_f^{m+1} + k^2 \hat{p}_f^{m+1} = 0 \qquad \text{in } (-\infty, 0),$$

whose solution is given by $\hat{p}_f^{m+1}(x,k) = P^{m+1}(k)\, e^{|k|x} + Q^{m+1}(k)\, e^{-|k|x}$. The boundedness assumption on the solution entails $Q^{m+1}(k) = 0$, thus

$$\hat{p}_f^{m+1}(x,k) = P^{m+1}(k)\, e^{|k|x}, \tag{13}$$

and the value of $P^{m+1}(k)$ is determined uniquely by the interface condition $(10)_4$

$$-2\mu_f\,\partial_x \hat{u}_1^{m+1} + \hat{p}_f^{m+1} - \alpha_f\,\hat{u}_1^{m+1} = \hat{p}_p^m + \alpha_f\,\eta_1\,\partial_x \hat{p}_p^m. \tag{14}$$

Similarly, the equation for the Darcy pressure reads, for all k,

$$-\eta_1\,\partial_{xx}\hat{p}_p^{m+1} + \eta_2\,k^2 \hat{p}_p^{m+1} = 0 \qquad \text{in } (0, +\infty),$$

whose solution, due to the boundedness assumption, is given by

$$\hat{p}_p(x,k) = \Phi^{m+1}(k)\, e^{-\sqrt{\frac{\eta_2}{\eta_1}}|k|x}, \tag{15}$$

where the value of $\Phi^{m+1}(k)$ is determined uniquely by the interface condition $(11)_2$

$$\hat{p}_p^{m+1} - \alpha_p\,\eta_1\,\partial_x \hat{p}_p^{m+1} = -2\mu_f\,\partial_x \hat{u}_1^{m+1} + \hat{p}_f^{m+1} + \alpha_p\,\hat{u}_1^{m+1}. \tag{16}$$

In order to write the fluid component of the Robin interface conditions $(10)_4$ and $(11)_2$ in terms of the sole pressure, we need to express the interface velocity $\hat{u}_1$ as a function of $\hat{p}_f$.
From (10), the first equation of the fluid problem in the x direction, after applying the Fourier transform in the y direction, reads

$$\partial_{xx}\hat{u}_1^{m+1} - k^2 \hat{u}_1^{m+1} = \frac{k}{\mu} P^{m+1}(k)\, e^{|k|x} \tag{17}$$

having noticed that $\partial_x \hat{p}_f^{m+1} = |k| P^{m+1}(k)\, e^{|k|x}$. Due to the boundedness assumption, the homogeneous solution of this equation is $\hat{u}_{1,hom}^{m+1}(x,k) = A^{m+1}(k)\, e^{|k|x}$ for suitable $A^{m+1}(k)$. As the right-hand side of (17) is a solution to the homogeneous equation, the solution to the complete equation is given by

$$\hat{u}_1^{m+1}(x,k) = \left(A^{m+1}(k) + \frac{x}{2\mu_f}\, P^{m+1}(k)\right) e^{|k|x}. \tag{18}$$

Inserting (13), (15) and (18) into (14) and (16), and using the fact that $\partial_x \hat{p}_p^{m+1} = -|k|\sqrt{\frac{\eta_2}{\eta_1}}\Phi^{m+1}(k)\, e^{-|k|x}$, we get

$$\begin{aligned} -(\alpha_f + 2\mu_f\,|k|)\; A^{m+1}(k) &= (1 - \alpha_f\,\eta_p\,|k|)\; \Phi^m(k) && \text{in } x = 0 \\ (1 + \alpha_p\,\eta_p\,|k|)\; \Phi^m(k) &= (\alpha_p - 2\mu_f\,|k|)\; A^{m-1}(k) && \text{in } x = 0. \end{aligned}$$

As a consequence, we have $|A^{m+1}(k)| = \rho(\alpha_f, \alpha_p, k)|A^{m-1}(k)|$, and in general $|A^{2m}(k)| = \rho^m(\alpha_f, \alpha_p, k)|A^0(k)|$, where $\rho(\alpha_f, \alpha_p, k)$ is given by (12). □

We want now to characterize optimal parameters $\alpha_f, \alpha_p > 0$ that ensure the convergence of the algorithm for all relevant frequencies. In particular, such parameters must ensure that $\rho(\alpha_f, \alpha_p, k) < 1$ for all $k \in [k_{min}, k_{max}]$. (Notice that the special choice $\alpha_p = \alpha_f$ always guarantees the convergence of the algorithm.)

3.4. **Optimization of the Robin parameters α_p and α_f.** We focus here on the choice of the parameters α_p and α_f and their optimization. We are interested in a range of frequencies $0 < k_{min} \leq |k| \leq k_{max}$. Considering the symmetry of $g(\alpha_f, \alpha_p, k)$ as a function of k, in the following we restrict ourselves to the case $k > 0$ without loss of generality. Ideally, the optimal parameters force the reduction factor $\rho(\alpha_p, \alpha_f, k)$ to be identically zero for all k, so that convergence is attained in a number of iterations equal to the number of subdomains (two, in the case at hand).
The optimal parameters can be easily devised from (12)

$$\alpha_p^{exact}(k) = 2\mu_f\, k \qquad\qquad \alpha_f^{exact}(k) = \frac{1}{\eta_p\, k}, \tag{19}$$

but they are unfortunately not viable. In fact, they both depend on the frequency k, and their back transforms in the physical space are either introducing an imaginary coefficient which multiplies a first order tangential derivative ($\alpha_p^{exact}(k)$) or result in a nonlocal operator ($\alpha_f^{exact}(k)$).

3.4.1. *Low-order Taylor approximation.* The first possible approach resides in using approximations based on low-order Taylor expansions of the optimal values (19), a choice that proved very effective when applied to the coupling of heterogeneous problems (see, e.g. [26]). Expanding the exact values, one around $k = k_{min}$ and the other around $k = k_{max}$, namely

$$\alpha_p^1 = \alpha_p^{exact}(k_{min}) = 2\mu_f\, k_{min} \qquad\qquad \alpha_f^1 = \alpha_f^{exact}(k_{max}) = \frac{1}{\eta_p\, k_{max}} \tag{20}$$

or

$$\alpha_p^2 = \alpha_p^{exact}(k_{max}) = 2\mu_f\, k_{max} \qquad\qquad \alpha_f^2 = \alpha_f^{exact}(k_{min}) = \frac{1}{\eta_p\, k_{min}},$$

guarantees exact convergence of the algorithm for the minimal and maximal frequency. Notice that if the minimal frequency is $k_{min} = 0$, only the first combination is viable, and corresponds to a Neumann-Robin iterative algorithm. Moreover, whenever $k_{min} > 0$, a little algebraic manipulation shows that $\rho(\alpha_f^1, \alpha_p^1, k) = \rho(\alpha_f^2, \alpha_p^2, k)$, for all $k \in [k_{min}, k_{max}]$.

Although the minimal and maximal frequencies are treated exactly, a Taylor expansion offers no control on the effective convergence rate of the algorithm, which is given by the maximum over all the relevant frequencies. As a function of $k \geq 0$, $g(\alpha_f, \alpha_p, k)$ is continuous, it has two positive roots $k_1 = (\alpha_f \eta_p)^{-1}$ and $k_2 = \alpha_p/(2\mu_f)$, and a local maximum in

$$k_* = \frac{\alpha_p - \alpha_f}{2\mu_f + \alpha_f\alpha_p\eta_p} + \sqrt{\left(\frac{\alpha_p - \alpha_f}{2\mu_f + \alpha_f\alpha_p\eta_p}\right)^2 + \frac{1}{2\mu_f\eta_p}}.$$

Rolle's theorem allows us to conclude that k_* lies between the zeros k_1, k_2 and that $g(\alpha_f, \alpha_p, k_*) > 0$. Finally, it can be easily shown that $0 < g(\alpha_f, \alpha_p, k_*) < 1$, independently of the values of α_f and α_p. In the case of the Taylor expansion, the zeros are in k_{min} and k_{max}, and the convergence of the Optimized Schwarz Method is then guaranteed. Moreover, a little algebra shows that the maximum is attained at

$$k_* = \frac{k_{min}k_{max} - \frac{1}{2\mu_f\eta_p}}{k_{min} + k_{max}} + \sqrt{\left(\frac{k_{min}k_{max} - \frac{1}{2\mu_f\eta_p}}{k_{min} + k_{max}}\right)^2 + \frac{1}{2\mu_f\eta_p}}\,. \tag{21}$$

and the effective convergence rate is then given by $\rho_{eff} = \rho(k_*)$.

Notice that using a first-order Taylor expansion would just recover $\alpha_p^{exact}(k)$ and, at the same time, provide an approximation for $\alpha_f^{exact}(k) \sim \frac{2}{\eta_p\, k_{max}} - \frac{1}{\eta_p\, k_{max}^2}\, k$ which suffers from the same drawback as $\alpha_p^{exact}(k)$ of introducing an imaginary coefficient in the physical space. The presence of such first-order term in the Taylor expansion of $\alpha_f^{exact}(k)$ makes therefore the use of higher-order expansions pointless.

3.4.2. *The classical min-max approach.* The classical approach in Optimized Schwarz literature consists in optimizing the parameters α_p and α_f by minimizing the convergence rate over all the relevant frequencies of the problem: this amounts to solve the min-max problem

$$\min_{\alpha_f, \alpha_p \in \mathbb{R}^+} \max_{k \in [k_{min}, k_{max}]} \rho(\alpha_f, \alpha_p, k). \tag{22}$$

The standard strategy in the literature is to either search for the optimized parameter on the diagonal $\alpha_f = \alpha_p$ (known as one-sided Robin conditions, that use the same coefficient for both sides of the interface), or minimize the effective convergence rate for (α_f, α_p) free to move in the positive quadrant of $\mathbb{R}^2$ (two-sided Robin conditions, that use different coefficients on the two sides of the interface). Usually, the first approach is simpler but provides less effective results than the latter, which, in return, can be in general pretty complicated to solve. By exploiting the problem characteristics, we can position ourselves halfway between the two approaches, and reduce problem (22) to a one parameter minimization along a curve in the positive quadrant. In the specific, from (19), we observe that the product of the optimal values $\alpha_f^{exact}(k)$ and $\alpha_p^{exact}(k)$ is constant and equals $2\mu/\eta_p$. We exploit such peculiarity of the problem (not occurring when the Optimized Schwarz Methods are used on homogeneous decomposition, see e.g. [22]), and restrict our search for optimized parameters along the curve

$$\alpha_f\, \alpha_p = \frac{2\mu_f}{\eta_p}. \tag{23}$$

Notice that such curve is the subset of the (α_f, α_p) upper-quadrant where the roots k_1 and k_2, of the convergence rate ρ coincide. The following result holds for the optimal values $\alpha_f^{exact}(k)$ and $\alpha_p^{exact}(k)$.

Lemma 3.1. *For any given $k \in (0, +\infty)$,*

$$\nabla\rho(\alpha_f^{exact}(k), \alpha_p^{exact}(k), k) = 0\,.$$

Moreover, the point $(\alpha_f^{exact}(k), \alpha_p^{exact}(k))$ is an absolute minimum.

Proof. The expression of the convergence rate $\rho(\alpha_f, \alpha_p, k)$ depends on the sign of the numerator in (12). We omit the dependence on k, we recall from (19) that $\alpha_f^{exact}(k) = \frac{1}{\eta_p\, k}$ and $\alpha_p^{exact}(k) = 2\mu_f\, k$, and we identify 4 regions in the (α_f, α_p) upper-right quadrant:

(1) for $\alpha_f < \dfrac{1}{\eta_p\, k}$ and $\alpha_p < 2\mu_f\, k$, $\quad \rho(\alpha_f, \alpha_p) = \left(\dfrac{2\mu_f\, k - \alpha_p}{2\mu_f\, k + \alpha_f}\right)\cdot\left(\dfrac{1 - \alpha_f\, \eta_p\, k}{1 + \alpha_p\, \eta_p\, k}\right) =: \rho_1(\alpha_f, \alpha_p)$;

(2) for $\alpha_f < \dfrac{1}{\eta_p\, k}$ and $\alpha_p \geq 2\mu_f\, k$, $\quad \rho(\alpha_f, \alpha_p) = \left(\dfrac{\alpha_p - 2\mu_f\, k}{2\mu_f\, k + \alpha_f}\right)\cdot\left(\dfrac{1 - \alpha_f\, \eta_p\, k}{1 + \alpha_p\, \eta_p\, k}\right) = -\rho_1(\alpha_f, \alpha_p)$;

(3) for $\alpha_f \geq \dfrac{1}{\eta_p\, k}$ and $\alpha_p \geq 2\mu_f\, k$, $\quad \rho(\alpha_f, \alpha_p) = \left(\dfrac{\alpha_p - 2\mu_f\, k}{2\mu_f\, k + \alpha_f}\right)\cdot\left(\dfrac{\alpha_f\, \eta_p\, k - 1}{1 + \alpha_p\, \eta_p\, k}\right) = \rho_1(\alpha_f, \alpha_p)$;

(4) for $\alpha_f \geq \dfrac{1}{\eta_p\, k}$ and $\alpha_p < 2\mu_f\, k$, $\quad \rho(\alpha_f, \alpha_p) = \left(\dfrac{2\mu_f\, k - \alpha_p}{2\mu_f\, k + \alpha_f}\right)\cdot\left(\dfrac{\alpha_f\, \eta_p\, k - 1}{1 + \alpha_p\, \eta_p\, k}\right) = -\rho_1(\alpha_f, \alpha_p)$.

The gradient of $\rho_1(\alpha_f, \alpha_p)$ is given by

$$\nabla\rho_1(\alpha_f, \alpha_p) \;=\; \begin{bmatrix} -\dfrac{1 + 2\mu_f\, \eta_p\, k^2}{1 + \alpha_p\, \eta_p\, k}\cdot\dfrac{2\mu_f\, k - \alpha_p}{(2\mu_f\, k + \alpha_f)^2} \\ -\dfrac{1 + 2\mu_f\, \eta_p\, k^2}{(1 + \alpha_p\, \eta_p\, k)^2}\cdot\dfrac{1 - \alpha_f\, \eta_p\, k}{(2\mu_f\, k + \alpha_f)^2} \end{bmatrix}.$$

Thus, for a generic k, $\nabla\rho_1(\alpha_f, \alpha_p) = 0$ in $\alpha_f = \frac{1}{\eta_p\, k}$ and $\alpha_p = 2\mu_f\, k$, while its sign behaves like

$$sign(\nabla\rho_1(\alpha_f, \alpha_p)) = sign \begin{bmatrix} \alpha_p - 2\mu_f\, k \\ \alpha_f\, \eta_p\, k - 1 \end{bmatrix}.$$

Owing to the definition of $\rho(\alpha_f, \alpha_p)$ in the 4 regions of the (α_f, α_p) upper-right quadrant, we have

(1) for $\alpha_f < \dfrac{1}{\eta_p\, k}$, $\alpha_p < 2\mu_f\, k$, $\quad \partial_{\alpha_f}\rho(\alpha_f, \alpha_f) < 0$, $\quad$ and $\quad \partial_{\alpha_p}\rho(\alpha_f, \alpha_p) < 0$;

(2) for $\alpha_f < \dfrac{1}{\eta_p\, k}$, $\alpha_p > 2\mu_f\, k$, $\quad \partial_{\alpha_f}\rho(\alpha_f, \alpha_P) < 0$, $\quad$ and $\quad \partial_{\alpha_p}\rho(\alpha_f, \alpha_p) > 0$;

(3) for $\alpha_f > \dfrac{1}{\eta_p\, k}$, $\alpha_p > 2\mu_f\, k$, $\quad \partial_{\alpha_f}\rho(\alpha_F, \alpha_P) > 0$, $\quad$ and $\quad \partial_{\alpha_p}\rho(\alpha_f, \alpha_p) > 0$;

(4) for $\alpha_f > \dfrac{1}{\eta_p\, k}$, $\alpha_p < 2\mu_f\, k$, $\quad \partial_{\alpha_f}\rho(\alpha_f, \alpha_p) > 0$, $\quad$ and $\quad \partial_{\alpha_p}\rho(\alpha_f, \alpha_p) < 0$.

Thus, the point $(\alpha_f, \alpha_p) = \left(\frac{1}{\eta_p\, k}\,,\, 2\mu_f\, k\right)$ is a minimum for $\rho(\alpha_f, \alpha_f)$. In addition, since $\rho(\alpha_f, \alpha_f) \geq 0$ and $\rho\left(\frac{1}{\eta_p\, k}\,,\, 2\mu_f\, k\right) = 0$, the minimum is absolute. □

Lemma 3.1 guarantees that, for any given k, the minimum of the convergence rate with respect to (α_f, α_p) lies on the hyperbola (23). The following proposition provides the solution of the optimization procedure along it.

Proposition 3.2. *The solution of the min-max problem*

$$\min_{\alpha_f\alpha_p=\frac{2\mu_f}{\eta_p}} \max_{k\in[k_{min},k_{max}]} \rho(\alpha_f,\alpha_p,k) \tag{24}$$

is given by the pair

$$\begin{aligned} \alpha_f^* &= \frac{1-2\mu_f\eta_p\,k_{min}k_{max}}{\eta_p(k_{min}+k_{max})} + \sqrt{\left(\frac{1-2\mu_f\eta_p\,k_{min}k_{max}}{\eta_p(k_{min}+k_{max})}\right)^2+\frac{2\mu_f}{\eta_p}} \\ \alpha_p^* &= -\frac{1-2\mu_f\eta_p\,k_{min}k_{max}}{\eta_p(k_{min}+k_{max})} + \sqrt{\left(\frac{1-2\mu_f\eta_p\,k_{min}k_{max}}{\eta_p(k_{min}+k_{max})}\right)^2+\frac{2\mu_f}{\eta_p}} \end{aligned} \tag{25}$$

Moreover, $\rho(\alpha_f^*,\alpha_p^*,k)<1$ *for all* $k\in[k_{min},k_{max}]$.

Proof. From Lemma 3.1 we know that, regardless where the maximum with respect to k is, the minimum with respect to (α_f,α_p) is along the hyperbola (23). A simple algebra shows that the convergence rate of the Optimized Schwarz Method along (23) reads

$$\rho(\alpha_f,k)=\frac{2\mu_f}{\eta_p}\left(\frac{\eta_p\alpha_f\,k-1}{2\mu_f k+\alpha_f}\right)^2. \tag{26}$$

The function in (26) is always positive and has a minimum in $k=\frac{1}{\eta_p\alpha_f}$, where it vanishes. Since it is continuous, its maximum is attained in one end of the interval $[k_{min},k_{max}]$:

$$\max_{k\in[k_{min},k_{max}]}\rho(\alpha_f,k) \;=\; \max\left\{\rho(\alpha_f,k_{min})\,,\,\rho(\alpha_f,k_{max})\right\}. \tag{27}$$

Moreover, being

$$\partial_{\alpha_f}\rho=\frac{4\mu_f}{\eta_p}\,\frac{2\mu_f\eta_p k^2+1}{(2\mu_f k+\alpha_f)^3}\,(\eta_p\alpha_f k-1)\,,$$

it is immediate to observe that for all $k\in[k_{min},k_{max}]$, $\rho(\alpha_f,k)$ is decreasing for $\alpha_f<\dfrac{1}{\eta_p k}$ and increasing for $\alpha_f>\dfrac{1}{\eta_p k}$. In particular, we have:

$$\rho(0,k_{min})>\rho(0,k_{max}), \qquad \rho\left(\frac{1}{\eta_p k_{max}},k_{min}\right)>\rho\left(\frac{1}{\eta_p k_{max}},k_{max}\right)=0$$

$$\lim_{\alpha_f\to\infty}\frac{\rho(\alpha_f,k_{min})}{\rho(\alpha_f,k_{max})}<1, \qquad \rho\left(\frac{1}{\eta_p k_{min}},k_{max}\right)>\rho\left(\frac{1}{\eta_p k_{min}},k_{min}\right)=0,$$

and we can observe that

$$\max\left\{\rho(\alpha_f,k_{min})\,,\,\rho(\alpha_f,k_{max})\right\}=\begin{cases}\rho(\alpha_f,k_{min}) & \text{for } \alpha_f<\alpha_f^*\\ \rho(\alpha_f,k_{max}) & \text{for } \alpha_f\geq\alpha_f^*\end{cases}$$

where $\alpha_f^*>0$ is the value at which the convergence rate exhibits equioscillation between the minimal and maximal frequency, i.e.,

$$\rho(\alpha_f^*,k_{min})=\rho(\alpha_f^*,k_{max})\,. \tag{28}$$

Simple algebraic manipulations show that finding the optimal value of α_f that satisfies (28) is equivalent to solving the following algebraic equation

$$\alpha_f^2+2\alpha_f\frac{2\mu_f\eta k_{min}k_{max}-1}{\eta(k_{min}+k_{max})}-\frac{2\mu_f}{\eta}=0\,, \tag{29}$$

whose positive solution α_f^* is given in (25). The expression for α_p^* in (25) is obtained by replacing α_f^* into (23). To guarantee that $\rho(\alpha_f^*, k) < 1$ for all $k \in [k_{min}, k_{max}]$, since both (27) and (28) hold, we just have to prove that either $\rho(\alpha_f^*, k_{min}) < 1$ or $\rho(\alpha_f^*, k_{max}) < 1$. First, notice that $\rho(\alpha_f^*, k) < 1$ if and only if

$$\left(\sqrt{\frac{2\mu_f}{\eta_p}}\frac{1-\eta_p\alpha_f^* k}{2\mu_f k+\alpha_f^*}-1\right)\left(\sqrt{\frac{2\mu_f}{\eta_p}}\frac{1-\eta_p\alpha_f^* k}{2\mu_f k+\alpha_f^*}+1\right)<0\,.$$

This inequality can be equivalently rewritten as

$$2\mu_f(\eta_p^2(\alpha_f^*)^2k^2+1)-\eta_p(4\mu_f^2k^2+(\alpha_f^*)^2+8\mu_f\alpha_f^*k)<0\,.$$

Using the expression of $(\alpha_f^*)^2$ from (29) and after a few simplifications, we obtain

$$-(1-2\mu_f\eta_p k_{min}k_{max})(1-2\mu_f\eta_p k^2)-4\mu_f\eta_p k(k_{min}+k_{max})<0\,.$$

It is straightforward to see that if we set, e.g., $k = k_{min}$ we find

$$-1-4\mu_f^2\eta_p k_{min}^3k_{max}-2\mu_f\eta_p k_{min}(k_{min}+k_{max})<0$$

which is obviously true. □

Remark 3.1. (i) *The ratio α_f^*/α_p^* only depends on the physical coefficients μ_f, η_p, and on the mesh size h. In fact, from equations* (25)*, we observe that*

$$\alpha_f^*-\alpha_p^*=2\,\frac{1-2\mu_f\eta_p\,k_{min}k_{max}}{\eta_p(k_{min}+k_{max})},$$

whose sign is ruled by the sign of the numerator. In particular, in the case $k_{min} = \pi/L$ (L being the length of the interface Γ) and $k_{max} = \pi/h$, we have

$$\alpha_f^*<\alpha_p^* \quad \text{if} \quad h<\frac{2\mu_f\eta_p\,\pi^2}{L} \quad \text{and} \quad \alpha_f^*>\alpha_p^* \quad \text{if} \quad h>\frac{2\mu_f\eta_p\,\pi^2}{L}. \tag{30}$$

(ii) *In the limit $h \to 0$, the convergence rate becomes $\rho(\alpha_f^0, \alpha_p^0, k)$, where*

$$\alpha_f^0=-\frac{2\mu_f\pi}{L}+\sqrt{\left(\frac{2\mu_f\pi}{L}\right)^2+\frac{2\mu_f}{\eta_p}}\,,\qquad \alpha_p^0=\frac{2\mu_f\pi}{L}+\sqrt{\left(\frac{2\mu_f\pi}{L}\right)^2+\frac{2\mu_f}{\eta_p}}, \tag{31}$$

entailing $\alpha_f^0 < \alpha_p^0$. This is not surprising: in fact, when $h \to 0$, $k_{max} \to \infty$ and $\lim_{k\to\infty}\rho(\alpha_f, \alpha_p, k) = \alpha_f/\alpha_p$. Thus, the larger the maximal frequency supported by the numerical grid, the larger α_p with respect to α_f to guarantee that the reduction factor is below 1.

3.4.3. *Minimization of the mean convergence rate.* Both the Taylor expansion and the equioscillation approach ensure that the Optimized Schwarz algorithm is convergent in its iterative form. However, when the Optimized Schwarz Method is used as a preconditioner for a Krylov method to solve the interface problem, these two choices do not necessarily guarantee the fastest convergence. A common feature of the Taylor expansion and the equioscillation approach is that the amount of frequencies showing a not so small convergence rate is not negligible (see Figure 2). In this section we present an alternative approach: by relaxing the constraint on the effective convergence rate, we look for parameters that ensure a better convergence for a larger number of frequencies in the error.
We still look for α_f and α_p along the curve (23) and we restrict ourselves to the set

$$\mathcal{A}_f=\{\alpha_f>0\,:\,\rho(\alpha_f,k)\le 1\quad \forall k\in[k_{min},k_{max}]\}\,. \tag{32}$$

Notice that the convergence of the Robin-Robin method in its iterative form would be ensured only in the case the inequality in the definition of $\mathcal{A}_f$ is strict. However, from the previous section we know that there can be at most one frequency whose corresponding convergence rate equals 1, either in k_{min} or in k_{max}. When the Optimized Schwarz Method is used as a preconditioner for a Krylov method, the latter can handle isolated problems in the spectrum. This last approach is actually the most popular in the literature (see, e.g., [21, 17, 25]).

Lemma 3.2. *The set $\mathcal{A}_f$ is one of the following intervals.*

(1) *If $\sqrt{2\mu_f\eta_p}k_{min} - 1 > 0$,*

$$\mathcal{A}_f = \left(0, \sqrt{\frac{2\mu_f}{\eta_p}} \min\left(\frac{\sqrt{2\mu_f\eta_p}k_{min}+1}{\sqrt{2\mu_f\eta_p}k_{min}-1}, \frac{\sqrt{2\mu_f\eta_p}k_{max}+1}{\sqrt{2\mu_f\eta_p}k_{max}-1}\right)\right] \tag{33}$$

(2) *If $\sqrt{2\mu_f\eta_p}k_{max} - 1 < 0$,*

$$\mathcal{A}_f = \left[\sqrt{\frac{2\mu_f}{\eta_p}} \max\left(-\frac{\sqrt{2\mu_f\eta_p}k_{min}-1}{\sqrt{2\mu_f\eta_p}k_{min}+1}, -\frac{\sqrt{2\mu_f\eta_p}k_{max}-1}{\sqrt{2\mu_f\eta_p}k_{max}+1}\right), +\infty\right) \tag{34}$$

(3) *If $\sqrt{2\mu_f\eta_p}k_{min} - 1 < 0$ and $\sqrt{2\mu_f\eta_p}k_{max} - 1 > 0$,*

$$\mathcal{A}_f = \left(0, \sqrt{\frac{2\mu_f}{\eta_p}}\frac{\sqrt{2\mu_f\eta_p}k_{max}+1}{\sqrt{2\mu_f\eta_p}k_{max}-1}\right] \cap \left[-\sqrt{\frac{2\mu_f}{\eta_p}}\frac{\sqrt{2\mu_f\eta_p}k_{min}-1}{\sqrt{2\mu_f\eta_p}k_{min}+1}, +\infty\right) \tag{35}$$

(4) *If $\sqrt{2\mu_f\eta_p}k_{min} - 1 = 0$,*

$$\mathcal{A}_f = \left(0, \sqrt{\frac{2\mu_f}{\eta_p}}\frac{\sqrt{2\mu_f\eta_p}k_{max}+1}{\sqrt{2\mu_f\eta_p}k_{max}-1}\right] \tag{36}$$

(5) *If $\sqrt{2\mu_f\eta_p}k_{max} - 1 = 0$,*

$$\mathcal{A}_f = \left[-\sqrt{\frac{2\mu_f}{\eta_p}}\frac{\sqrt{2\mu_f\eta_p}k_{min}-1}{\sqrt{2\mu_f\eta_p}k_{min}+1}, +\infty\right). \tag{37}$$

Proof. The condition $\rho(\alpha_f, k) \leq 1$ can be equivalently reformulated as

$$\begin{aligned}&\left(\alpha_f\sqrt{\eta_p}\left(\sqrt{2\mu_f\eta_p}k+1\right)+\sqrt{2\mu_f}\left(\sqrt{2\mu_f\eta_p}k-1\right)\right)\\ &\left(\alpha_f\sqrt{\eta_p}\left(\sqrt{2\mu_f\eta_p}k-1\right)-\sqrt{2\mu_f}\left(\sqrt{2\mu_f\eta_p}k+1\right)\right) \leq 0\,.\end{aligned}$$

The term $\sqrt{2\mu_f\eta_p}k+1$ is always positive, while $\sqrt{2\mu_f\eta_p}k-1$ may change its sign, so we must discuss different cases. Owing to (27) we are ensured that $\rho(\alpha_f, k) \leq 1$ for all $k \in [k_{min}, k_{max}]$ provided the inequality holds in both k_{min} and k_{max}, thus we consider only both $k = k_{min}$ and $k = k_{max}$.
(i) If $\sqrt{2\mu_f\eta_p}k_{min} - 1 > 0$, then also $\sqrt{2\mu_f\eta_p}k_{max} - 1 > 0$, so that $\mathcal{A}_f$ is the set (33).
(ii) If $\sqrt{2\mu_f\eta_p}k_{max} - 1 < 0$, also $\sqrt{2\mu_f\eta_p}k_{min} - 1 < 0$, and $\mathcal{A}_f$ is the set (34).
(iii) If $\sqrt{2\mu_f\eta_p}k_{min} - 1 < 0$, then either $\sqrt{2\mu_f\eta_p}k_{max} - 1 < 0$, in which case we obtain again (34), or $\sqrt{2\mu_f\eta_p}k_{max} - 1 > 0$ and $\mathcal{A}_f$ is the set (35).
(iv) If $\sqrt{2\mu_f\eta_p}k_{max} - 1 > 0$, either $\sqrt{2\mu_f\eta_p}k_{min} - 1 > 0$, in which case we obtain (33), or
$\sqrt{2\mu_f\eta_p}k_{min} - 1 < 0$ and we get (35).
(v) If $\sqrt{2\mu_f\eta_p}k_{min} - 1 = 0$, $k_{max} > k_{min} = 1/\sqrt{2\mu_f\eta_p}$ so that $\sqrt{2\mu_f\eta_p}k_{max} - 1 > 0$.

Thus, $\mathcal{A}_f$ is characterized as (36).
(vi) Finally, if $\sqrt{2\mu_f\eta_p}k_{max}-1=0$, $k_{min}<k_{max}=\frac{1}{\sqrt{2\mu_f\eta_p}}$ so that $\sqrt{2\mu_f\eta_p}k_{min}-1<0$. Thus, $\mathcal{A}_f$ is the set (37). □

In order to improve the overall convergence for a Krylov method, we minimize, on the set $\mathcal{A}_f$, the expected value of $\rho(\alpha_f,k)$ in the interval $[k_{min},k_{max}]$:

$$E(\alpha_f) := \mathbb{E}[\rho(\alpha_f,k)] = \frac{1}{k_{max}-k_{min}}\int_{k_{min}}^{k_{max}} \rho(\alpha_f,k)\,dk\,. \tag{38}$$

Owing to (26), the expected value of $\rho(\alpha_f,k)$ in $[k_{min},k_{max}]$ can be explicitly computed with the help of a little calculus, and we have

$$E(\alpha_f) = \frac{1}{2\mu_f}\left(\alpha_f^2\eta_p + \frac{(\alpha_f\eta_p+2\mu_f)^2}{\eta_p(2\mu_f k_{max}+\alpha_f)(2\mu_f k_{min}+\alpha_f)} - \frac{\alpha_f(\alpha_f^2\eta_p+2\mu_f)}{\mu_f(k_{max}-k_{min})}\log\left(\frac{2\mu_f k_{max}+\alpha_f}{2\mu_f k_{min}+\alpha_f}\right)\right).$$

The function $E(\alpha_f)$ is continuous, positive (being the integral of a non-negative function), $E(0)=1/(2\mu_f\eta_p k_{min}k_{max})$, $\lim_{\alpha_f\to+\infty}E(\alpha_f)=+\infty$ and $\partial_{\alpha_f}E(0)<0$. Thus, $E(\alpha_f)$ has at least one (local) minimum $\alpha_f^{opt}<+\infty$ in $\mathcal{A}_f$ that may coincide with one of the extrema of $\mathcal{A}_f$ if the latter is a bounded set. In table 1 we report the optimization interval $\mathcal{A}_f$ and the resulting optimized parameter α_f^{opt} for different values of the problem coefficients μ_f and η_p. In addition, in Fig. 2 we plot the convergence rates, as a function of k, for the zero-order Taylor expansion (T), the solution (25) of the min-max problem via equioscillation (E), and α_f^{opt} (M), for two set of coefficients μ_f and η_p.

TABLE 1. Optimization interval $\mathcal{A}_f$ and optimized parameter α_f^{opt} for different values of the coefficients μ_f and η_p and $h=2^{-5}$. The column (m,M) reports the signs of $(2\mu_f\eta_p\,k_{min}-1)$ and $(2\mu_f\eta_p\,k_{max}-1)$, respectively, where $k_{min}=\pi$ and $k_{max}=\pi/h$.

μ_f	η_p	(m,M)	$\mathcal{A}_f$	α_f^{opt}
1	1	(+,+)	(0, 1.4342]	0.0357
1	1e-2	(-,+)	[5.4414, 16.2821]	5.4414
1	1e-4	(-,+)	[129.3895, 812.1057]	217.3489
1e-1	1	(+,+)	(0, 0.4676]	0.0364
1e-2	1	(-,+)	[0.0544, 0.1628]	0.0544
1e-1	1e-2	(-,+)	[3.3703, 7.0307]	3.3703
1e-1	1e-3	(-,+)	[12.9390, 81.2106]	21.7349
1e-1	1e-4	(-,-)	[43.4821,+∞)	195.9084

4. Numerical results

In this section we present some numerical tests to assess the performance of the Optimized Schwarz method. In particular, we focus on the effectiveness and robustness of the method with respect both to the mesh size h and to the physical parameters μ_f and η_p.

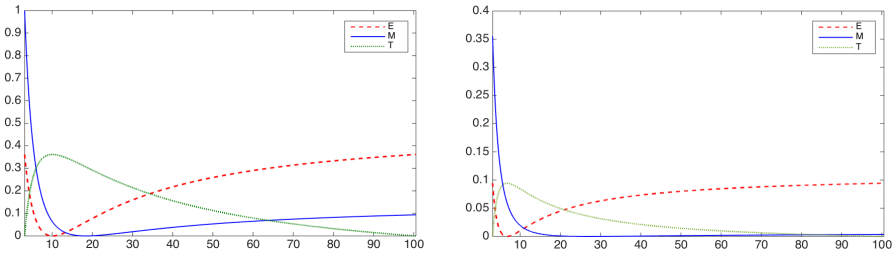

FIGURE 2. Convergence rates, as a function of k, for the parameters obtained through zero-order Taylor expansion (T, dotted line), the solution of the min-max problem via equioscillation (E, dashed line), and α_f^{opt} (M, solid line). Left: $\mu_f = 1$, $\eta_p =$ 1e-2, $h = 2^{-5}$. Right: $\mu_f =$ 1e-1, $\eta_p = 1$, $h = 2^{-5}$.

4.1. **Finite element discretization and algebraic form.** We consider a finite element discretization based on Taylor-Hood elements for the Stokes problem (see, e.g., [5]) and on quadratic Lagrangian elements for the scalar elliptic form of the Darcy equation. Let the indices I_f, I_p and Γ denote the internal degrees of freedom in Ω_f, Ω_p and on the interface. Let $\boldsymbol{\lambda}_p$ and $\boldsymbol{\lambda}_f$ be the vectors of components $\int_\Gamma \lambda_p \psi_i$ and $\int_\Gamma \lambda_f \psi_i$, where λ_p and λ_f are the interface variables $\lambda_p = p_p + \alpha_f(\boldsymbol{\eta}_p \nabla p_p \cdot \mathbf{n} - \mathbf{g}_p \cdot \mathbf{n})$ and $\lambda_f = -\mathbf{n} \cdot (2\mu_f \nabla^{\mathrm{s}} \mathbf{u}_f - p_f \boldsymbol{I}) \cdot \mathbf{n} + \alpha_p \mathbf{u}_f \cdot \mathbf{n}$ on Γ, and ψ_i is a suitable finite element basis function on Γ. Letting $M_{\Gamma\Gamma}$ be a mass matrix on Γ, we can write the algebraic form of the algorithm (8)-(9) as follows: given $\boldsymbol{\lambda}_p^0$, for $m \geq 1$ until convergence

1. solve the Stokes problem

$$\begin{pmatrix} (A_f^{\mu_f})_{I_f I_f} & (A_f^{\mu_f})_{I_f \Gamma} & (G_f)_{I_f} \\ (A_f^{\mu_f})_{\Gamma I_f} & (A_f^{\mu_f})_{\Gamma\Gamma} + \alpha_f M_{\Gamma\Gamma} & (G_f)_{\Gamma} \\ (G_f)_{I_f}^T & (G_f)_{\Gamma}^T & 0 \end{pmatrix} \begin{pmatrix} \mathbf{u}_{s,I_f}^m \\ \mathbf{u}_{s,\Gamma}^m \\ \mathbf{p}_f^m \end{pmatrix} = \begin{pmatrix} \mathbf{f}_{s,I_f} \\ \mathbf{f}_{s,\Gamma} \\ \mathbf{0} \end{pmatrix} - \begin{pmatrix} \mathbf{0} \\ \boldsymbol{\lambda}_p^{m-1} \\ \mathbf{0} \end{pmatrix} \tag{39}$$

   where $\mathbf{u}_{s,\Gamma}$ is the vector of the degrees of freedom of the normal velocity on Γ;
2. compute

$$\boldsymbol{\lambda}_f^m = \boldsymbol{\lambda}_p^{m-1} + (\alpha_f + \alpha_p) M_{\Gamma\Gamma} \mathbf{u}_{s,\Gamma}^m \tag{40}$$

3. solve the Darcy problem

$$\begin{pmatrix} (A_p^{\eta_p})_{I_p I_p} & (A_p^{\eta_p})_{I_p \Gamma} \\ (A_p^{\eta_p})_{\Gamma I_p} & (A_p^{\eta_p})_{\Gamma\Gamma} + \alpha_p^{-1} M_{\Gamma\Gamma} \end{pmatrix} \begin{pmatrix} \mathbf{p}_{p,I_p}^m \\ \mathbf{p}_{p,\Gamma}^m \end{pmatrix} = \begin{pmatrix} \mathbf{g}_{p,I_p} \\ \mathbf{g}_{p,\Gamma} \end{pmatrix} + \alpha_p^{-1} \begin{pmatrix} \mathbf{0} \\ \boldsymbol{\lambda}_f^m \end{pmatrix} \tag{41}$$

   where $\mathbf{p}_{p,\Gamma}$ is the vector of the degrees of freedom of the pressure on Γ;
4. compute

$$\boldsymbol{\lambda}_p^m = \left(1 + \frac{\alpha_f}{\alpha_p}\right) M_{\Gamma\Gamma} \mathbf{p}_{p,\Gamma}^m - \frac{\alpha_f}{\alpha_p} \boldsymbol{\lambda}_f^m. \tag{42}$$

Let $R_{f,\Gamma}$ be the algebraic restriction operator that to the Stokes velocity and pressure in Ω_f associates the Stokes normal velocity on the interface Γ. Moreover, let $R_{p,\Gamma}$ be the algebraic restriction operator that to the Darcy pressure in Ω_p

associates the Darcy pressure on the interface Γ. Then, we can introduce the discrete Robin-to-Dirichlet operators

$$\begin{aligned} S_f &= R_{f,\Gamma} \begin{pmatrix} (A_f^{\mu_f})_{I_f I_f} & (A_f^{\mu_f})_{I_f \Gamma} & (G_f)_{I_f} \\ (A_f^{\mu_f})_{\Gamma I_f} & (A_f^{\mu_f})_{\Gamma\Gamma} + \alpha_f M_{\Gamma\Gamma} & (G_f)_{\Gamma} \\ (G_f)_{I_f}^T & (G_f)_{\Gamma}^T & 0 \end{pmatrix}^{-1} R_{f,\Gamma}^T \\ S_p &= \alpha_p^{-1} R_{p,\Gamma} \begin{pmatrix} (A_p^{\eta_p})_{I_p I_p} & (A_p^{\eta_p})_{I_p \Gamma} \\ (A_p^{\eta_p})_{\Gamma I_p} & (A_p^{\eta_p})_{\Gamma\Gamma} + \alpha_p^{-1} M_{\Gamma\Gamma} \end{pmatrix}^{-1} R_{p,\Gamma}^T . \end{aligned}$$

Simple algebraic computations allow to reinterpret (39)-(42) as a Gauss-Seidel iteration to solve the interface linear system

$$A_{RR} \begin{pmatrix} \boldsymbol{\lambda}_f \\ \boldsymbol{\lambda}_p \end{pmatrix} = \begin{pmatrix} -(\alpha_f + \alpha_p) M_{\Gamma\Gamma} \mathbf{f}_\Gamma \\ \left(1 + \frac{\alpha_f}{\alpha_p}\right) M_{\Gamma\Gamma} \mathbf{g}_\Gamma \end{pmatrix} \tag{43}$$

where

$$A_{RR} = \begin{pmatrix} -I & I - (\alpha_f + \alpha_p) M_{\Gamma\Gamma} S_f \\ \frac{\alpha_f}{\alpha_p} I - \left(1 + \frac{\alpha_f}{\alpha_p}\right) M_{\Gamma\Gamma} S_p & I \end{pmatrix} \tag{44}$$

and $\mathbf{f}_\Gamma$ and $\mathbf{g}_\Gamma$ are vectors depending on the data of the problem. A_{RR} is non-symmetric and indefinite. In fact, if N_Γ is the number of rows of $\boldsymbol{\lambda}_f$ (or, equivalently, $\boldsymbol{\lambda}_p$) and $(\mathbf{x}, \mathbf{y})$ is an arbitrary non-null vector in $\mathbb{R}^{2N_\Gamma}$, then, denoting by $(\cdot,\cdot)_2$ and $\|\cdot\|_2$ the Euclidean scalar product and norm, we obtain

$$\left(\mathbf{x}^T, \mathbf{y}^T\right) A_{RR} \begin{pmatrix} \mathbf{x} \\ \mathbf{y} \end{pmatrix} = \|\mathbf{y}\|_2^2 - \|\mathbf{x}\|_2^2 + \left(1 + \frac{\alpha_f}{\alpha_p}\right) \left((\mathbf{x}, \mathbf{y})_2 - \alpha_p \mathbf{x}^T M_{\Gamma\Gamma} S_f \mathbf{y} - \mathbf{y}^T M_{\Gamma\Gamma} S_p \mathbf{x}\right),$$

whose sign may be either positive or negative.

4.2. **Test 1.** We assess the effectiveness of the Optimized Schwarz method on a model problem with known analytic solution. The computational domains are $\Omega_f = (0,1)\times(1,2)$ and $\Omega_p = (0,1)\times(0,1)$ separated by the interface $\Gamma = (0,1)\times\{1\}$. The computational grids are uniform, structured, made of triangles and characterized by mesh size $h = 2^{-(s+2)}$ with $s = 1, \ldots, 6$. We set η_p constant (assuming $\eta_1 = \eta_2$), $\alpha_{BJ} = 1$, $k_{min} = \pi$ and $k_{max} = \pi/h$. The boundary conditions and the forcing terms are such that the exact solution is $\mathbf{u}_f = (\sqrt{\mu_f \eta_p},\, \alpha_{BJ} x)$, $p_f = 2\mu_f(x + y - 1) + (3\eta_p)^{-1}$, $p_p = (-\alpha_{BJ} x(y-1) + y^3/3 - y^2 + y)/\eta_p + 2\mu_f x$. We solve the interface system (43) using GMRES ([36]) with tolerance 1e-9 on the relative residual starting the iterations from $(\boldsymbol{\lambda}_f,\, \boldsymbol{\lambda}_p)^T = \mathbf{0}$.

In Figs. 3–4 we plot the values of α_f and α_p computed using the three approaches studied in Sects. 3.4.1–3.4.3 and the corresponding number of GMRES iterations for different values of μ_f, η_p and h. The method based on low-order Taylor approximation is not very effective, since the number of iterations grows significantly in some cases, especially for small values of the physical parameters. The coefficients computed both with equioscillation and with the mean minimization criterion seem to guarantee robustness with respect to h, i.e., the iteration counts appear to stabilize as the mesh size becomes reasonable in terms of accuracy of the solution, and this behaviour remains evident as $h \to 0$. However, there is still dependence on the value of the physical parameters. Finally, notice that the parameters obtained by equioscillation obey the inequalities (30), i.e., α_f is larger than α_p if the mesh size h is large enough compared to the physical parameters of the problem, while α_f

becomes smaller than α_p if h is taken small enough. Although an analytic expression is not available for α_f and α_p in the case of mean minimization, we can infer from the graphs that they behave in an analogous way as concerns their mutual magnitude.

In table 2 we show the effective convergence rate $\rho_{max} = \max_{k\in[k_{min},k_{max}]} \rho(\alpha_f, \alpha_p, k)$, the mean convergence rate $E(\alpha_f, \alpha_p) = (k_{max} - k_{min})^{-1} \int_{k_{min}}^{k_{max}} \rho(\alpha_f, \alpha_p, k)\, dk$ and the iteration count for different values of μ_f and η_p, $h = 2^{-5}$ and the three choices of the optimal parameters: low-order Taylor expansion (T) (20), equioscillation (E) (25), and mean minimization (M). We can observe that minimizing the effective convergence rate is not necessary a winning strategy. In general, minimizing the mean convergence rate is providing better results when an iterative method is used to solve the interface problem, even in the case when the effective convergence rate equals 1.

TABLE 2. Effective convergence rate ρ_{max}, mean convergence rate $E(\alpha_f, \alpha_p)$ and iteration count for different values of μ_f and η_p, $h = 2^{-5}$ and the three choices of α_f, α_p: low-order Taylor expansion (T), equioscillation (E), and mean minimization (M).

μ_f	η_p	α_f	α_p	ρ_{max}	$E(\alpha_f, \alpha_p)$	Iter	
		0.0099	6.2832	0.0116	0.0026	8	(T)
1	1	0.1622	12.3285	0.0116	0.0089	8	(E)
		0.0357	56.0435	0.0395	0.0009	8	(M)
		0.9947	6.2832	0.3613	0.1363	22	(T)
1	1e-2	9.9150	20.1714	0.3613	0.2320	18	(E)
		5.4414	36.7552	1.0000	0.0729	14	(M)
		99.4718	6.2832	0.2414	0.1581	46	(T)
1	1e-4	258.1914	77.4619	0.2414	0.0853	30	(E)
		217.3489	92.0180	0.3472	0.0775	26	(M)
		0.0099	0.6283	0.0945	0.0239	12	(T)
1e-1	1	0.1484	1.3477	0.0945	0.0706	12	(E)
		0.0364	5.4896	0.3549	0.0089	10	(M)
		0.0099	0.0628	0.3613	0.1363	22	(T)
1e-2	1	0.0992	0.2017	0.3613	0.2320	18	(E)
		0.0544	0.3676	1.0000	0.0729	14	(M)
		0.9947	0.6283	0.4806	0.2740	38	(T)
1e-1	1e-2	4.8415	4.1309	0.4806	0.2249	24	(E)
		3.3703	5.9342	1.0000	0.1313	20	(M)
		9.9472	0.6283	0.2414	0.1581	46	(T)
1e-1	1e-3	25.8191	7.7462	0.2414	0.0853	30	(E)
		21.7349	9.2018	0.3472	0.0775	26	(M)
		99.4718	0.6283	0.0429	0.0286	32	(T)
1e-1	1e-4	201.6164	9.9198	0.0429	0.0143	32	(E)
		195.9084	10.2089	0.0456	0.0143	32	(M)

Finally, in Fig. 5 we consider four possible combinations of μ_f and η_p and $h = 2^{-5}$ and we show the number of iterations for a range of values α_f and α_p. In all cases, the optimal coefficients devised by minimizing the convergence rate either fall in the regions of minimum number of iterations or are in the closest ones to it.

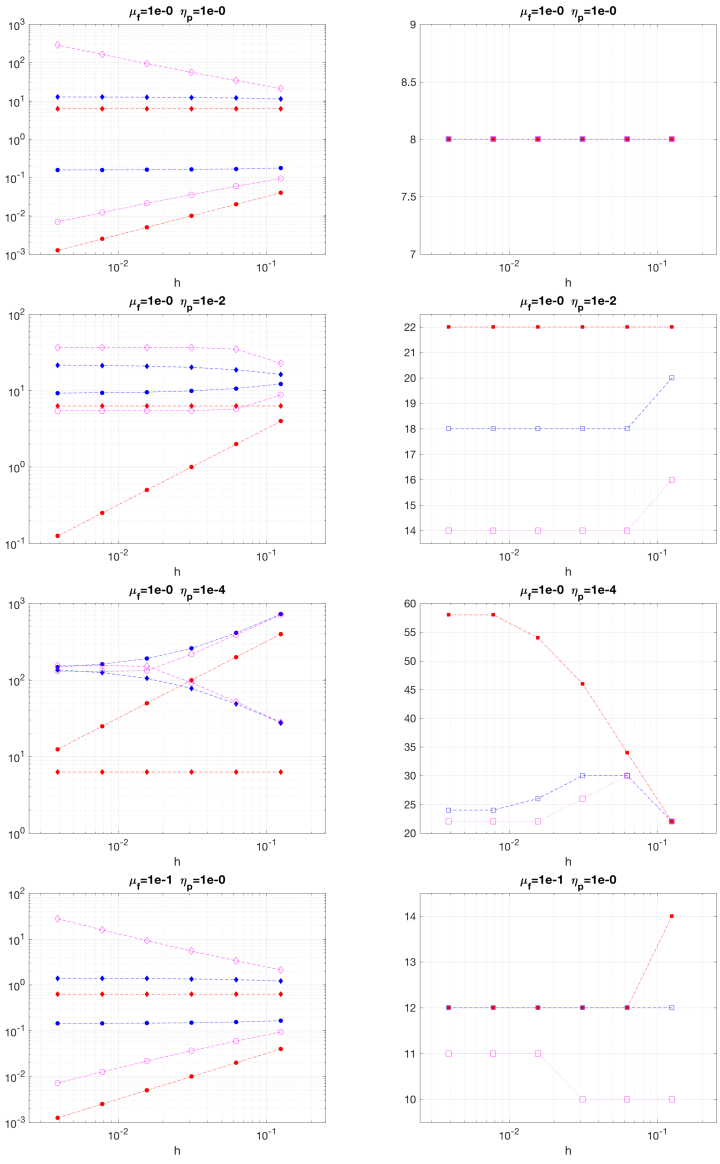

FIGURE 3. Left: parameters α_f (circles) and α_p (diamonds) versus h for different values of μ_f and η_p. Right: corresponding number of iterations versus h. Red lines: low-order Taylor expansion; blue: equioscillation; magenta: mean minimization.

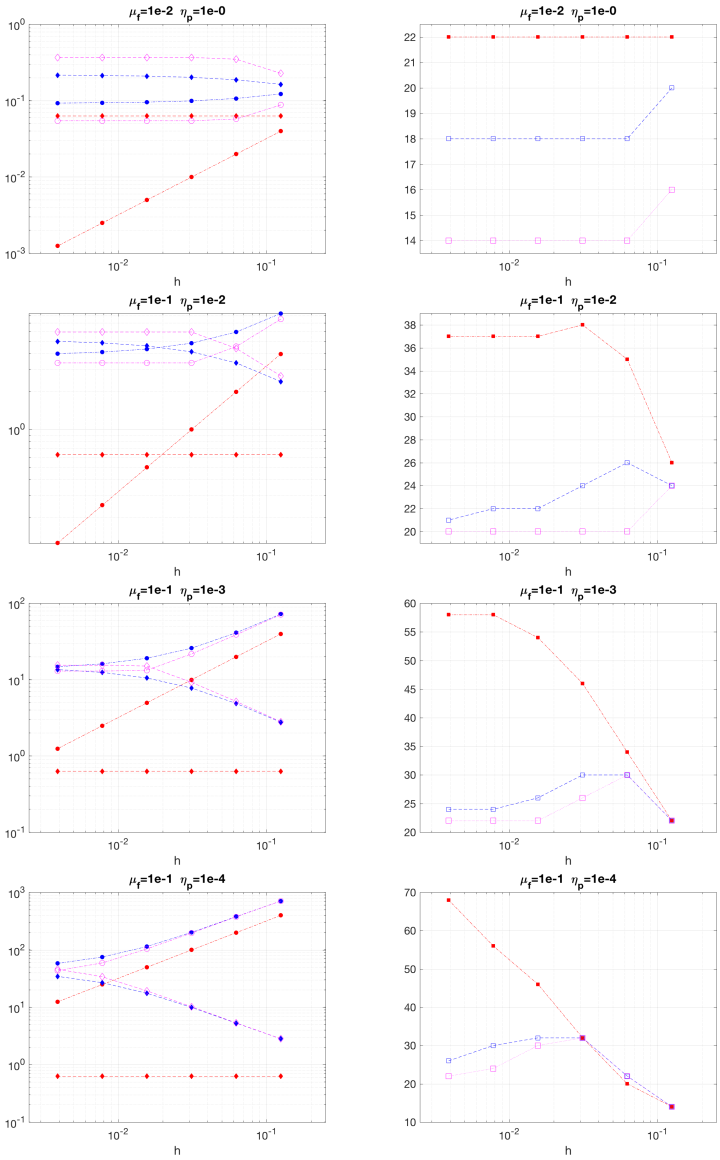

FIGURE 4. Left: parameters α_f (circles) and α_p (diamonds) versus h for different values of μ_f and η_p. Right: corresponding number of iterations versus h. Red lines: low-order Taylor expansion; blue: equioscillation; magenta: mean minimization.

4.3. **Test 2.** We simulate a 2D cross-flow membrane filtration problem similarly to [29]. The fluid domain is $\Omega_f = (0, 0.015) \times (0.0025, 0.0075)$ m, the porous medium domain is $\Omega_p = (0.0035, 0.0105) \times (0, 0.0025)$ m and the interface is $\Gamma = (0.0035, 0.0105) \times 0.0025$ m. The boundary conditions are set as follows: on $\Gamma_f^{in} = \{0\} \times (0.0025, 0.0075)$ we impose the parabolic inflow velocity profile $\mathbf{u}_f =$

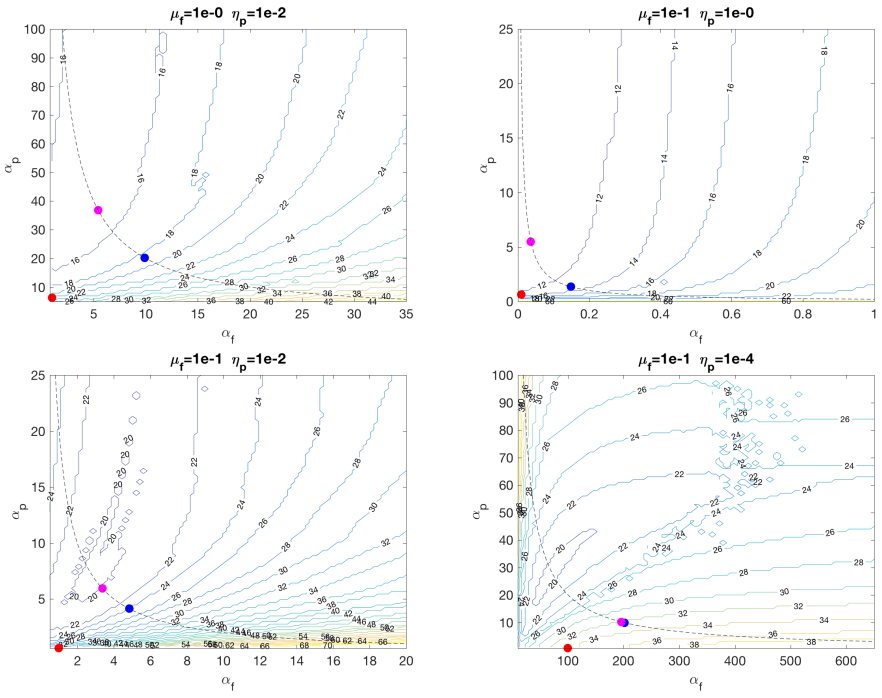

FIGURE 5. Number of iterations for $h = 2^{-5}$ and different values of α_f and α_p. The dotted line represents the curve $\alpha_f\alpha_p = 2\mu_f/\eta_p$ (23). The red circle corresponds to (α_f, α_p) computed using the low-order Taylor expansion (20), the blue circle to the case of equioscillation (25) and the magenta circle to the mean minimization.

$(-16000y^2 + 160y - 0.3, 0)$ m/s; on $\Gamma_f^{out} = \{0.015\} \times (0.00625, 0.0075)$, $(2\mu\nabla^{\mathrm{s}}\mathbf{u}_f - p_f\boldsymbol{I})\cdot\mathbf{n} = \mathbf{0}$ kg/(m·s); on $\partial\Omega_f\backslash(\Gamma_f^{in}\cup\Gamma_f^{out}\cup\Gamma)$, $\mathbf{u}_f = \mathbf{0}$ m/s; on $\Gamma_p^b = (0.0035, 0.0105)\times\{0\}$, $p_p = 0$ kg/(m·s); on $\partial\Omega_p \setminus (\Gamma_p^b \cup \Gamma)$, $\mathbf{u}_p \cdot \mathbf{n} = 0$ m/s. Since gravitational effects are neglected, both $\mathbf{f}_f$ and $\mathbf{g}_p$ are null. The fluid has density 1000 kg/m^3 and dynamic viscosity 0.001 kg/(m·s). The permeability is either $\boldsymbol{K}_1$ = 1e-6 $diag(1,1)$ m^2 or $\boldsymbol{K}_2$ = 1e-12 $diag(1,1)$ m^2. Finally, $\alpha_{BJ} = 1$. Using $X_f = 0.005$ m and $U_f = 0.1$ m/s for adimensionalization, we obtain $\mu_f = 0.002$, $\eta_p = 20$ for $\boldsymbol{K}_1$ and η_p = 2e-5 for $\boldsymbol{K}_2$. Table 3 reports the coefficients α_f and α_p together with the number of GMRES iterations required to converge to the tolerance 1e-9 on the relative residual for the two different values of the permeability. We can see that the mean minimization approach guarantees convergence in a number of iterations almost independent of the computational grid and it better performs than both the low-order Taylor and the equioscillation methods at least is η_p is quite large. The computed solutions are shown in Figs. 6 and 7.

5. CONCLUSIONS

In this paper an Optimized Schwarz method for the Stokes-Darcy problem was studied. Different strategies have been provided to practically compute optimal

TABLE 3. Parameters α_f, α_p and GMRES iterations for the cases of low-order Taylor expansion, equioscillation and mean minimization. Meshes with $h = 2^{-(2+s)}$. dofs is the number of interface unknowns. Top: $\mu_f = 0.002$, $\eta_p = 20$. Bottom: $\mu_f = 0.002$, $\eta_p =$ 2e-5.

s	dofs	α_f	α_p	iter	α_f	α_p	iter	α_f	α_p	iter
		(low-order Taylor)			(equioscillation)			(mean minimization)		
1	50	1.99e-03	8.98e-03	21	9.11e-03	2.19e-02	18	5.18e-03	3.86e-02	13
2	98	9.95e-04	8.98e-03	21	8.43e-03	2.37e-02	17	3.34e-03	5.99e-02	13
3	194	4.97e-04	8.98e-03	21	8.10e-03	2.47e-02	17	3.16e-03	6.33e-02	13
4	386	2.49e-04	8.98e-03	21	7.94e-03	2.52e-02	17	3.16e-03	6.33e-02	13

s	dofs	α_f	α_p	iter	α_f	α_p	iter	α_f	α_p	iter
		(low-order Taylor)			(equioscillation)			(mean minimization)		
1	50	1.99e+03	8.98e-03	10	3.65e+03	5.48e-01	10	1.99e+03	1.01e-01	10
2	98	9.95e+02	8.98e-03	10	1.90e+03	1.05e-01	10	9.95e+02	2.01e-01	10
3	194	4.97e+02	8.98e-03	12	9.73e+02	2.06e-01	12	4.97e+02	4.02e-01	12
4	386	2.49e+02	8.98e-03	14	4.92e+02	4.06e-01	14	2.49e+02	8.04e-01	14

parameters for the Robin interface conditions to guarantee the convergence of the method. The methods we propose take into account both the physical parameters typical of this coupled problem (i.e., the fluid viscosity and the permeability of the porous medium) and the size h of the computational grid used for simulations. Previous results ([16]) showed that for a fixed computational mesh and fluid viscosity and permeability tending to zero, convergence of the Robin-Robin method was guaranteed if $\alpha_f > \alpha_p$. However, [10] proved that geometric convergence could be obtained in some cases for an appropriate choice of $\alpha_f < \alpha_p$. The analysis carried out in this paper helps to clarify the issue of the relative size of the parameters by clearly highlighting that their values may significantly change depending not only on the physical parameters of the problem but also on the computational grid used for the finite element approximation. In particular, (30) shows that, if the product of the physical parameters is small enough compared to h, then $\alpha_f > \alpha_p$ guarantees an optimal convergence of the Robin-Robin algorithm, while for fine enough meshes, α_p may be taken larger than α_f. Finally, in this paper the Robin-Robin method is reinterpreted as an iterative method to solve a suitable interface linear system (43) for which Krylov space methods can be used to enhance convergence.

ACKNOWLEDGEMENTS

The first author acknowledges partial funding from the European Union Seventh Framework Programme (FP7/2007-2013) under grand agreement no. 294229. The second author acknowledges the support from the Basque Government through the BERC 2014-2017 program, and from the Spanish Ministry of Economics and Competitiveness MINECO through the BCAM Severo Ochoa excellence accreditation SEV-2013-0323

x

REFERENCES

[1] A. Alonso-Rodriguez and L. Gerardo-Giorda. New non-overlapping domain decomposition methods for the time-harmonic Maxwell system. *SIAM J. Sci. Comput.*, 28(1):102–122, 2006.

[2] J. Bear. *Hydraulics of Groundwater*. McGraw-Hill, New York, 1979.

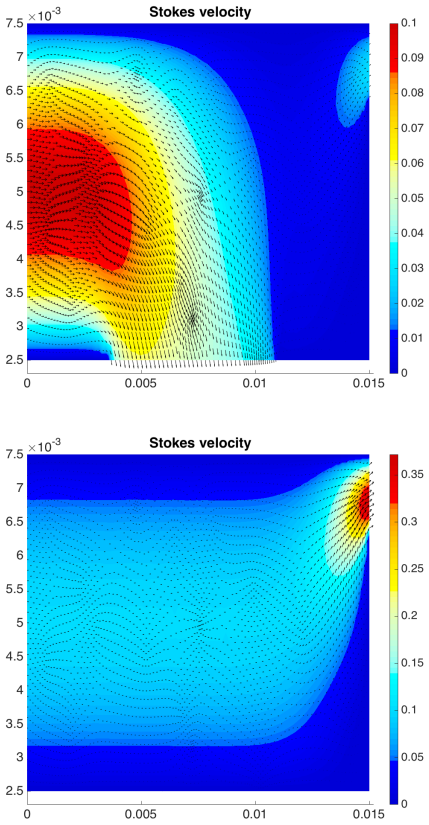

FIGURE 6. Stokes velocity for $\boldsymbol{K}_1 = $ 1e-6 $diag(1,1)$ m^2 (left) and $\boldsymbol{K}_2 = $ 1e-12 $diag(1,1)$ m^2 (right).

[3] J. Bear and Y. Bachmat. *Introduction to Modeling of Transport Phenomena in Porous Media*. Kluwer Academic Publisher, Dordrecht (The Netherlands), 1991.

[4] G.S. Beavers and D.D. Joseph. Boundary conditions at a naturally permeable wall. *J. Fluid Mech.*, 30:197–207, 1967.

[5] D. Boffi, F. Brezzi, and M. Fortin. *Mixed Finite Element Methods and Applications*. Springer, Berlin and Heidelberg, 2013.

[6] A. Caiazzo, V. John, and U. Wilbrandt. On classical iterative subdomain methods for the Stokes-Darcy problem. *Comput. Geosci.*, 18:711–728, 2014.

[7] Y. Cao, M. Gunzburger, X. Hu, F. Hua, X. Wang, and W. Zhao. Finite element approximations for Stokes-Darcy flow with Beavers-Joseph interface conditions. *SIAM J. Numer. Anal.*, 47(6):4239–4256, 2010.

[8] Y. Cao, M. Gunzburger, F. Hua, and X. Wang. Coupled Stokes-Darcy model with Beavers-Joseph interface boundary conditions. *Comm. Math. Sci.*, 8(1):1–25, 2010.

[9] Ph. Charton, F. Nataf, and F. Rogier. Méthode de décomposition de domaine pour l'équation d'advection-diffusion. *C. R. Acad. Sci.*, 313(9):623–626, 1991.

[10] W. Chen, M. Gunzburger, F. Hua, and X. Wang. A parallel Robin-Robin domain decomposition method for the Stokes-Darcy system. *SIAM J. Numer. Anal.*, 49(3):1064–1084, 2011.

[11] P. Collino, G. Delbue, P. Joly, and A. Piacentini. A new interface condition in the non-overlapping domain decomposition for the Maxwell equations. *Comput. Methods Appl. Mech. Engrg.*, 148:195–207, 1997.

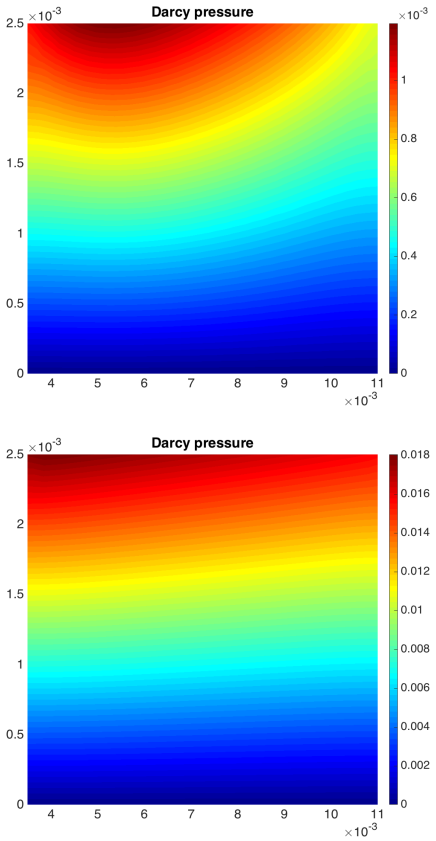

FIGURE 7. Darcy pressure for $\boldsymbol{K}_1 = $ 1e-6 $diag(1,1)$ m^2 (left) and $\boldsymbol{K}_2 = $ 1e-12 $diag(1,1)$ m^2 (right).

[12] Q. Deng. An analysis for a nonoverlapping domain decomposition iterative procedure. *SIAM J. Sci. Comput.*, 18:1517–1525, 1997.

[13] M. Discacciati. *Domain Decomposition Methods for the Coupling of Surface and Groundwater Flows*. PhD thesis, École Polytechnique Fédérale de Lausanne, Switzerland, 2004.

[14] M. Discacciati, E. Miglio, and A. Quarteroni. Mathematical and numerical models for coupling surface and groundwater flows. *Appl. Numer. Math.*, 43:57–74, 2002.

[15] M. Discacciati and A. Quarteroni. Navier-Stokes/Darcy coupling: modeling, analysis, and numerical approximation. *Rev. Mat. Complut.*, 22(2):315–426, 2009.

[16] M. Discacciati, A. Quarteroni, and A. Valli. Robin-Robin domain decomposition methods for the Stokes-Darcy coupling. *SIAM J. Numer. Anal.*, 45(3):1246–1268, 2007.

[17] V. Dolean, M.J. Gander, and L. Gerardo-Giorda. Optimized Schwarz methods for Maxwell's equations. *SIAM J. Sci. Comput.*, 31(3):2193–2213, 2009.

[18] V. Dolean and F. Nataf. An Optimized Schwarz Algorithm for the compressible Euler equations. In O.B. Widlund and D.E. Keyes, editors, *Domain Decomposition Methods in Science and Engineering XVI*, pages 173–180, Berlin and Heidelberg, 2007. Springer.

[19] O. Dubois. Optimized Schwarz methods with Robin conditions for the advection-diffusion equation. In O.B. Widlund and D.E. Keyes, editors, *Domain Decomposition Methods in Science and Engineering XVI*, pages 181–188, Berlin and Heidelberg, 2007. Springer.

[20] B. Engquist and H.-K. Zhao. Absorbing boundary conditions for domain decomposition. *Appl. Numer. Math.*, 27(4):341–365, 1998.

[21] M. Gander, F. Magoulès, and F. Nataf. Optimized Schwarz methods without overlap for the Helmholtz equation. *SIAM J. Sci. Comput.*, 21(1):38–60, 2002.
[22] M.J. Gander. Optimized Schwarz methods. *SIAM J. Numer. Anal.*, 44(2):699–731, 2006.
[23] M.J. Gander, L. Halpern, and F. Magoulès. An optimized Schwarz method with two-sided Robin transmission conditions for the Helmholtz equation. *Int. J. Numer. Meth. Fluids*, 55(2):163–175, 2007.
[24] L. Gerardo-Giorda, F. Nobile, and C. Vergara. Analysis and optimization of Robin-Robin partitioned procedures in fluid-structure interaction problems. *SIAM J. Numer. Anal.*, 48(6):2091–2116, 2010.
[25] L. Gerardo-Giorda and M. Perego. Optimized Schwarz methods for the bidomain system in electrocardiology. *M2AN*, 75(2):583–608, 2013.
[26] L. Gerardo-Giorda, M. Perego, and A. Veneziani. Optimized Schwarz coupling of bidomain and monodomain models in electrocardiology. *M2AN*, 45(2):309–334, 2011.
[27] V. Girault and B. Rivière. DG approximation of coupled Navier-Stokes and Darcy equations by Beaver-Joseph-Saffman interface condition. *SIAM J. Numer. Anal.*, 47:2052–2089, 2009.
[28] T. Hagstrom, R.P. Tewarson, and A. Jazcilevich. Numerical experiments on a domain decomposition algorithm for nonlinear elliptic boundary value problems. *Appl. Math. Lett.*, 1(3):299–302, 1988.
[29] N.S. Hanspal, A.N. Waghode, V. Nassehi, and R.J. Wakeman. Development of a predictive mathematical model for coupled Stokes/Darcy flows in cross-flow membrane filtration. *Chemical Engineering Journal*, 149:132–142, 2009.
[30] W. Jäger and A. Mikelić. On the boundary conditions at the contact interface between a porous medium and a free fluid. *Ann. Scuola Norm. Sup. Pisa Cl. Sci.*, 23:403–465, 1996.
[31] C. Japhet, F. Nataf, and F. Rogier. The optimized order 2 method. Application to convection-diffusion problems. *Future Generation Computer Systems*, 18(1):17–30, 2001.
[32] W.L. Layton, F. Schieweck, and I. Yotov. Coupling fluid flow with porous media flow. *SIAM J. Num. Anal.*, 40:2195–2218, 2003.
[33] P.L. Lions. On the Schwarz alternating method III: a variant for non-overlapping subdomains. In T.F. Chan, R. Glowinski, J. Périaux, and O. Widlund, editors, *Third International Symposium on Domain Decomposition Methods for Partial Differential Equations*, pages 202–231, Philadelphia, 1990. SIAM.
[34] F. Nataf and F. Rogier. Factorization of the convection-diffusion operator and the Schwarz algorithm. *Math. Models Meth. Appl. Sci.*, 5(1):67–93, 1995.
[35] A. Quarteroni and A. Valli. *Domain Decomposition Methods for Partial Differential Equations*. The Clarendon Press, Oxford University Press, New York, 1999.
[36] Y. Saad and M.H. Schultz. GMRES: a generalized minimal residual algorithm for solving nonsymmetric linear systems. *SIAM J. Sci. Stat. Comput.*, 7:856–869, 1986.
[37] P.G. Saffman. On the boundary condition at the interface of a porous medium. *Stud. Appl. Math.*, 1:93–101, 1971.
[38] B.F. Smith, P.E. Bjørstad, and W.D. Gropp. *Domain Decomposition: Parallel Multilevel Methods for Elliptic Partial Differential Equations*. Cambridge University Press, Cambridge, 1996.
[39] A. Toselli and O. Widlund. *Domain Decomposition Methods – Algorithms and Theory*, volume 34 of *Springer Series in Computational Mathematics*. Springer-Verlag, Berlin, 2005.

[1] Department of Mathematical Sciences, Loughborough University, Loughborough, UK

[2] BCAM – Basque Center for Applied Mathematics, Bilbao, Spain
E-mail address: M.Discacciati@lboro.ac.uk, lgerardo@bcamath.org